Impact of temporal beach grain size variability on aeolian sediment transport and topographic evolution in a microtidal environment

Antoine Lamy, Nicolas Robin, Thomas A.G. Smyth, Patrick Hesp, Camille René, Pierre Feyssat, Olivier Raynal, Bertil Hebert

Geomorphology 453 (2024) 109126

Contents lists available at ScienceDirect

Geomorphology

journal homepage: www.journals.elsevier.com/geomorphology

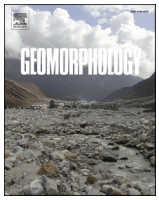

Impact of temporal beach grain size variability on aeolian sediment transport and topographic evolution in a microtidal environment

Antoine Lamy [a,*], Nicolas Robin [a], Thomas A.G. Smyth [b], Patrick A. Hesp [c], Camille René [a], Pierre Feyssat [a], Olivier Raynal [a], Bertil Hebert [a]

[a] CEFREM, UMR CNRS 5110, Université de Perpignan Via-Domitia, 66100 Perpignan, France
[b] Department of Biological and Geographical Sciences, School of Applied Sciences, University of Huddersfield, England, United Kingdom
[c] Beach and Dune Systems (BEADS) Laboratory, College of Science and Engineering, Flinders University, Bedford Park, South Australia 5041, Australia

ARTICLE INFO

Keywords:
Aeolian sand transport
Offshore wind
Beach grain size
Gulf of Lions

ABSTRACT

While the impact of the spatio/temporal variability of grain size on morphological beach state is reasonably well understood, relatively little is known on its impact at a scale of days/months on aeolian sediment transport. This study focuses on five short intensive wind events during which aeolian sediment transport measurements, beach surface sampling and elevation change surveys were carried out for 1 to 3 days, over a 16-month period on a microtidal beach dominated by offshore winds. Monthly observations show a high temporal variability in beach grain size in relation to the decoupling between hydrodynamic and aeolian processes, from medium sand after a marine storm and inundation of the beach, to very coarse sand after several weeks of storm-force winds. During each wind event, topographic change on the beach ranged from zero, to 0.55 m. The time scale of coarsening depended on the initial beach grain size and could be very fast when the beach was composed of medium sand (e.g. 388 μm sand changed to coarse sand of 547 μm in 40 h). In contrast, it took one month to transition from a coarse median beach grain size of 883 μm to a very coarse one of 1323 μm. This variability in grain size results in dramatically different rates of sediment flux. For example, during average wind speeds of 10 to 14 m/s the sediment flux when the beach was composed of medium sized sand ranged between 21 and 154 kg/m/h compared to 0.4 to 50 kg/m/h when the beach was composed of coarse and very coarse sized grains. Overall, this study highlights the importance of beach grain size variability on aeolian sediment transport and shows that for similar incident wind and climatic conditions aeolian sediment transport rates vary dramatically. The study demonstrates the importance of taking care when using a constant median grain size in the calculation of long-term aeolian sand transport on beaches with heterogeneous spatial and temporal beach grain size variability.

1. Introduction

Studies in coastal aeolian processes have identified multiple factors that limit sediment transport including surface moisture content, waves and tidal fluctuations (Bauer et al., 2009; He et al., 2022; Mountney and Russell, 2009; Schmutz and Namikas, 2018; Hallin et al., 2023). The fetch length (Dong et al., 2002; Bauer and Davidson-Arnott, 2003; Delgado-Fernandez, 2010; Schwarz et al., 2021), beach slope (Hardisty and Whitehouse, 1988; de Vries et al., 2012) and beach sand availability (Ruz and Anthony, 2008) are also factors to consider in the study of sand transport, as well as the presence of roughness elements such as vegetation (Buckley, 1987; Arens et al., 2001; Schwarz et al., 2021) and lag deposits (Van der Wal, 1998; de Vries et al., 2014). The characteristics of surface beach sediments can also influence the rate of sand flux (Bagnold, 1937), for example, aeolian sorting can coarsen the beach surface and create an armoured layer (Bagnold, 1937; Carter, 1976; Lancaster et al., 2002; Hoonhout and Vries, 2016; Field and Pelletier, 2018; Cohn et al., 2022; Uphues et al., 2022).

Globally, beaches present a wide range of granulometry from fine sand to boulders due to the local geology, tidal and wave actions, and sediment supply sources that in turn produce a diversity of beach morphologies (Bascom, 1951; Wright and Short, 1984; Bujan et al., 2019). Spatially, longshore variations in grain size at a landscape scale can be observed due to the distance from the sediment source (coarser near the source (e.g. estuary), finer away from it) (Aleman et al., 2015; Huisman et al., 2016). At a local scale, the same beach can present spatial and

* Corresponding author.
E-mail address: antoine.lamy.1@univ-perp.fr (A. Lamy).

https://doi.org/10.1016/j.geomorph.2024.109126
Received 25 August 2023; Received in revised form 22 February 2024; Accepted 29 February 2024
Available online 1 March 2024

temporal grain size variations due to hydrodynamic and wind forcing (Nordstrom, 1980; Moreira, 1988; Davidson-Arnott and Law, 1990; Medina et al., 1994; Prodger et al., 2016; Feyssat et al., 2022; Van IJzendoorn et al., 2022) causing cross-shore variation in grain size distribution between the upper beach and the nearshore zone (Aleman et al., 2015). It is frequently observed that during prolonged periods of strong winds, sediment sorting produces a coarser beach surface which decreases the saltation cascade effect and the amount of sediment transported (Davidson-Arnott and Law, 1990; Lancaster et al., 2002; Dong and Qian, 2006; Manukyan and Prigozhin, 2009; Strypsteen et al., 2021; Wang et al., 2021; Uphues et al., 2022). This is more pronounced in microtidal environments (Masselink and Pattiaratchi, 2001) where the low tidal range does not allow hydrodynamic processes (waves and tidal currents) to frequently mix the beach surface sediment. In an attempt to reduce this complexity, studies have often used a single grain size value to characterize their beach environment (Van IJzendoorn et al., 2022; Van IJzendoorn et al., 2023). However, relatively little attention has been devoted to assessing the impact of temporal grain size changes on aeolian transport rates, even though many beaches on mid-to high latitude coasts comprise a mixture of fine and coarse clastic materials. Calculating aeolian transport rates with greater accuracy has become necessary in the global context of coastline erosion, as it enhances the modelling of aeolian sediment transport on beaches, which acts as the primary source for the growth of foredunes and other dune types occurring adjacent to the shore (Hesp, 2024).

The aim of this study is to investigate the influence of the daily to monthly grain size variation on aeolian sediment transport that occurs on the backshore of a microtidal beach (Leucate, North-West Mediterranean coast), with large temporal grain size variations. The temporal evolution of the beach sedimentology was studied by analysing the environmental conditions (wind speed, wind direction and wave height) from January 2021 to April 2022. In addition, five field campaigns (1–3 days range), during the dominant field site wind direction (offshore) referred to as “events” were carried out to investigate the influence of the beach sedimentology on aeolian sand transport and topographic change.

2. Study area

The field site is located at Leucate Beach in the south of the Gulf of Lion (SE France, Mediterranean coast) (Fig. 1). It is a sand barrier (1.8 km long and 0.5 km mean width) with a low elevation dune system (4.5 m NGF, French Ordnance Datum in which 0 is close to mean sea level). This dune system was human-made and fixed by vegetation landward from the dune crest (Fig. 1c). The foredune and hind dune are topographically stable and only impacted by infrequent sediment deposition during onshore storms without rain and waves. The remnants of a fence have a limited effect on the transport of sand as it is located in the lee of the dune during offshore winds. No sand accumulation at the remnants of the fence was observed during our surveys. The mean beach width is around 40–50 m and the intertidal area is comprised of mega-cusps due to the prevailing crescentic nearshore bar system (Ferrer et al., 2010; Aleman et al., 2015). The backshore is flat and has a lower elevation (1 m NGF) between the dune toe (2.5 m NGF) and the berm (1.5 m NGF). Aleman et al. (2015) observed a median grain size (D_{50}) of 750 μm on the beach, but in this study we noted an average D_{50} ranging from 388 μm to 1323 μm.

The Gulf of Lion is a microtidal, wave-dominated environment. The tidal range is small (<0.3 m at mean spring tide) but large variations in sea water level can occur in response to wind forcing and atmospheric pressure fluctuations. Wave set-up can reach 1 m (Certain, 2002) under the combined action of storm surge and waves. Mean offshore significant wave heights (H_s) are generally small (H_s < 0.3 m for 75 % of the time and H_s < 1.5 m for 94 %), but can exceed >4 m during winter storms, and >7 m during the most energetic events (Aleman et al., 2015). A storm is locally defined when the H_s exceeds 2 m (Aleman et al., 2011; Mendoza et al., 2011) inducing overwash above the berm but without complete inundation of the beach. Complete inundation of the beach is observed when H_s is higher than 4 m with a water line located at the dune toe (Feyssat et al., 2022). The site is dominated by two main

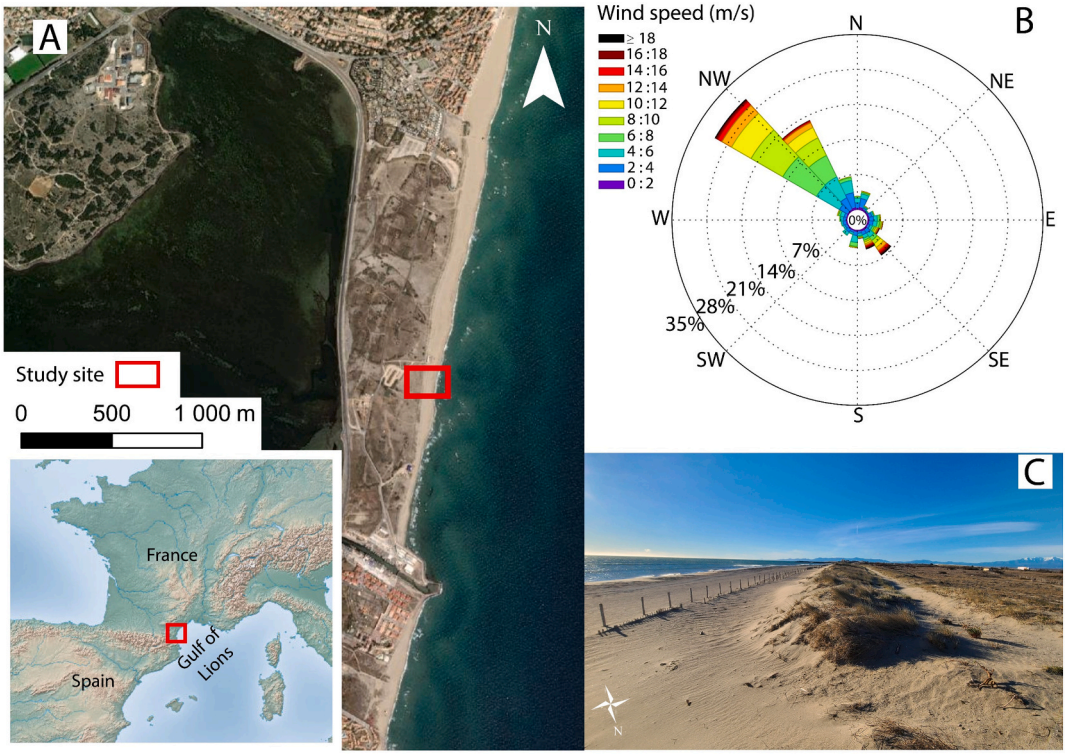

Fig. 1. (a) Location of the study area. (b) Wind rose at Cape Leucate station between 2015 and 2022. (c) Photograph looking southward along the foredune. The fence is composed only of wooden posts and will not inhibit the transport of sand.

wind orientations: NW offshore winds (71.6 % of the time with 17.5 % ≥ 10 m/s for the period January 2015 to April 2022), and E to SE onshore winds (28.6 % of the time) (Fig. 1b). Strong offshore winds often occur without precipitation and are predominantly recorded from autumn to spring to an strength up to 28 m/s for 10 to 30 days per year, with wind gusts up to 43 m/s. Onshore winds are more frequent during summer but associated with fair weather (low wind speeds). In winter onshore wind events are less frequent than offshore wind events but are typically very intense, with strong winds, high air humidity, rainfall and large waves. The regional wind pattern and dominance of offshore winds is due to the regional relief surrounded by two mountains chains (Pyrenees and central massif) and the global climatic circulation in the North Atlantic and Europe which often creates a pressure gradient in the Gulf of Lion.

3. Data and methods

This study is based on two temporal scales, annual and event (1 to 3 days). Environmental conditions (wind speed and direction at a meteorological station, 3 km north of the field site and wave height) were measured over a 16 month period from January 2021 to April 2022, to understand the sedimentology of the beach at the beginning of each field campaign (e.g. after a long offshore wind period or after marine storms). Five 1–3 day field campaigns were also conducted during dry, offshore wind storms termed "events" ("E"). During each event aeolian sediment transport, wind characteristics, beach grain size and topographic change were measured on the beach.

3.1. Annual scale survey

Meteorological measurements were provided by the Météo-France meteorological station on Cape Leucate, 3 km north of the study site and 42 m above sea level. Météo-France provided hourly Mean Wind ("MW") data defined as the maximum 10 min average wind speed per hour and Wind Gust data ("WG"), defined as the highest 1 s wind record per hour. Wave data was obtained from the Leucate wave buoy moored at a depth of 40 m and monitored by the Cerema, with the CANDHIS network (Cerema and Dreal, 2019). The wave data assessed backshore submersion based on two thresholds, H_s of 2 m for berm overwash and 4 m for beach inundation up to the dune toe, as observed in the field by Feyssat et al. (2022).

3.2. Events scale survey

3.2.1. Wind data

One ultrasonic anemometer (GILL WindSonic 4) was positioned on the dune crest at 2 m height (dune station, Fig. 2) during each of the five campaigns. This anemometer recorded wind direction at ±3° and wind speed with a range of 0 to 60 m/s at ±2 %. The wind was measured from the dune station at 1 Hz, then averaged over 1-minute intervals for graphical representation and 10 s for the calculation of the shear velocity (u*) during the sand transport measurements.

3.2.2. Topographic data

A kinematic differential global positioning system (Trimble R8s) was used to measure beach topography at the beginning and end of each event. The data accuracy (±0.02 m) was evaluated using control benchmarks on the beach. A topographic profile from the back dune to the swash zone was recorded with a spatial resolution of 1 m or less following the beach-dune morphology.

3.2.3. Grain size data

During the campaigns, several surface sediment samples were collected by scraping the beach surface (Nield et al., 2011) along the instrumental profile at the beginning of E1, E2 and E3, at the beginning, during and the end of E4, and at the beginning and the end of E5 (Table 1 and Fig. 2). They were not collected exactly in the same location for each Event, which is why they were spread throughout different zones around five meters each. For Events 1 and 2 only two and three samples were collected but the backshore is only 30 to 40 m wide which enables a reliable characterization of the beach granulometry. For Events 3, 4 and 5 the sample number was increased to improve the spatial characterization of the beach granulometry and because the backshore was slightly wider. Samples were dried and weighed to obtain sediment moisture values. All the campaigns took place on a dry beach (<1 %). While the beach was dry at the beginning of E5, moisture patches were observed as the campaign progressed. These were formed due to aeolian sediment erosion (Fig. 6c). The samples were analyzed using an AFNOR (Association Française de Normalisation) column of 22 sieves with class size between 10,000 to 50 μm to obtain the median particle size (D_{50}), by the Wentworth classification.

3.3. Sand trap design

Aeolian flux was measured during the five field campaigns using self-orienting, vertical-array sand traps modified from Hilton et al. (2017) at the beach berm crest (Fig. 2). A total of 24 aeolian sand transport recordings were made, called runs ("R"), each 15 min long. The traps were made from 38 × 38 mm square-sections of PVC and were mounted on a pivot pole allowing them to rotate and adjust their orientation depending on the wind direction. During each run, the heights of the traps were fixed, but the number and height of traps varied between events (synthesized in Table 1), as the number of traps available increased during the study. As recommended by Hilton et al. (2017), some minor modifications were made to the design of the sand trap. The pivot pole was installed 20 mm further downwind inside the traps to

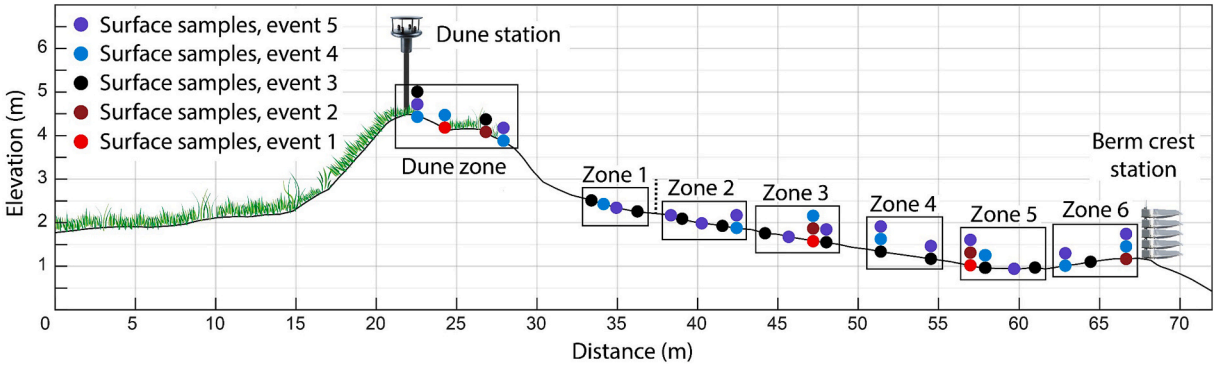

Fig. 2. Topographic profile across the beach and the foredune showing the surface samples separate in 6 different zones, for Event 1 (2021/02/01), Event 2 (2021/03/09), Event 3 (2022/01/05), Event 4 (2022/01/31 to 2022/02/02) and Event 5 (2022/03/31 to 2022/04/04). Remnant wooden fence posts are represented by the dotted line.

Table 1
Overview of data acquisition during the five events.

	Transport runs ("R")	Trap height (m)	Topographic data	Beach surface sample
Event 1 (2021/02/01)	R1 : 15:29 R2 : 16:10	R1/2 : 0.01-0.08-0.13-0.42	2021/02/01 10:30 and 16:15	2021/02/01 10:30
Event 2 (2021/03/09)	R3 : 11:15 R4 : 12:02 R5 : 12:49 R6 : 15:01 R7 : 15:40	R3/4/5/6/7 : 0.01 - 0.08 - 0.13 - 0.19 - 0.25 - 0.30 - 0.36 - 0.41 - 0.47 - 0.53	2021/03/09 10:45 and 17:15	2021/03/09 10:45
Event 3 (2022/01/04 to 2022/01/06)	01/05 { R8 : 14:02 R9 : 14:42	R8/9 : 0.01 - 0.08 - 0.13 - 0.19 - 0.25 - 0.30 - 0.36 - 0.41 - 0.47 - 0.53	2022/01/04 10:00 and 2022/01/06 09:00	2022/01/05 13:00
Event 4 (2022/01/31 to 2022/02/02)	01/31 { R10 : 09:32 R11 : 13:08 R12 : 17:03 02/01 { R13 : 04:50 R14 : 08:15 R15 : 12:29 R16 : 16:12 R17 : 23:10 02/02 { R18 : 00:04 R19 : 10:24	R10/11/12/14/15/16/19 : 0.01 - 0.04 - 0.08 - 0.14 - 0.20 - 0.25 - 0.31 - 0.37 - 0.42 - 0.48 - 0.53 - 0.72 R13/17/18 : 0.01 - 0.04 - 0.08 - 0.14 - 0.20 - 0.25 - 0.31 - 0.37 - 0.42 - 0.48 - 0.53 - 0.59	2022/01/31 09:00 and 11:00 2022/02/02	2022/01/31 09:00 2022/02/01 08:00 and 2022/02/02 11:00
Event 5 (2022/03/30 to 2022/04/04)	03/30 { R20 : 12:34 R21 : 14:18 04/01 { R22 : 15:58 R23 : 10:09 R24 : 12:17	R21/22/23/24 : 0.01 - 0.04 - 0.08 - 0.14 - 0.20 - 0.25 - 0.31 - 0.37 - 0.42 - 0.48 - 0.53 - 0.59	2022/03/30 16:30 and 2022/04/04 10:00	2022/03/30 16:30 and 2022/04/04 10:00

reduce the sediment loss due to grains bouncing out of the trap and for Event 4 and Event 5 instead of measuring 38 × 38 mm, the bottom trap was divided into two traps of 38 × 20 mm which reduced the errors in the calculation of sediment flux as described in Hilton et al. (2017) and Ellis et al. (2009).

3.4. Aeolian sand transport calculation

In order to calculate the sediment flux, the position of each trap was calculated using a geometric mean (Eq. (1)) where h_b was the bottom of the trap and h_t the top (Rasmussen and Mikkelsen, 1998; Namikas, 2003; Ellis et al., 2009).

$$Geometric\ Mean = \sqrt{h_t \times h_b} \tag{1}$$

To be consistent with the literature, the transport rates per trap were calculated in kg/m^2/h, then integrated to calculate total vertical sand flux using a non-linear least squares exponential decay function (Eq. (2)) that gives reliable results of sand flux Q_{tot} in kg/m/h with a and b are the regression coefficients (Ellis et al., 2009; Bauer and Davidson-Arnott, 2014; Poortinga et al., 2014; Swann et al., 2021).

$$Q_{tot} = \int_0^{+\infty} ae^{-bz}\, dz \tag{2}$$

3.5. Shear velocity calculation

Shear velocity u_* (Eq. (3)), was calculated using the law of the wall and Hsu's (1973) protocol by measuring wind at one elevation above the bed $u(z)$:

$$u(z) = \frac{u_*}{k} ln\left(\frac{z}{z_0}\right) \tag{3}$$

where k is the von Karman's constant equal to 0.4 and z_0 is the aerodynamic roughness approximate with the grain size d/30 define by Nikuradse (1933). The threshold shear velocity in Eq. (4) is commonly estimated with the Bagnold's (1937) equation:

$$u_{*t} = A\sqrt{\frac{\rho_s - \rho}{\rho} gd} \tag{4}$$

where A was considered equal to 0.085, assuming active saltation (Bagnold, 1937) and ρ_s the sediment density, u_* and u_{*t} were calculated at 10 s intervals for a good representation throughout each 15 min sediment trapping period (Section 3.3).

4. Results

4.1. Overview of the marine and aeolian conditions

4.1.1. Annual scale

The month before the first event (E1, 2021/02/01) was characterized by low-energy wave conditions (Fig. 3a), because of the strong dominance of offshore winds (80 % of the time). In this period MW were above 10 m/s 19 % of the time and WG were above 20 m/s 8 % of the time (Fig. 3b-c). The period between the first and second events (E1, 2021/02/01 to E2, 2021/03/09) was impacted by a strong marine storm (2021/02/22) with H_s of 4.6 m (Fig. 3a), that inundated the backshore. The dominant wind direction during this period was onshore (59 % of the time, Fig. 3b-c). In the April to September period before the third event (E3, 2022/02/02) the weather was fair with light winds and small waves (Fig. 3a-b-c), From October prior to E3, meteorological conditions were unsettled with many consecutive days and weeks of strong offshore winds where MW and WG exceeded 10 and 20 m/s respectively. The month between events three and four (E3, 2022/02/02 to E4, 2022/03/31) had a similar pattern to the previous weeks with a prevailing offshore wind where MW above 10 m/s occurred 33 % of the time, and WG were above 20 m/s 15 % of the time (Fig. 3b-c). The period between events four and five (E4, 2022/02/02 to E5, 2022/03/31) were dominated by onshore winds (60 % of the time, Fig. 3a) and a large 10 day long marine storm occurred between 2022/03/11 to 2022/03/21. H_s reached 4.9 m, inducing a total inundation of the backshore (Figs. 3a, 7a).

4.1.2. Event scale

During all the events, wave heights were small and water levels never exceeded the beach berm. This is because the strong offshore winds generated waves that propagated away from the study site (Feyssat et al., 2024). During the sand transport runs (R1 and R2) of E1, the mean wind speed was around 15 to 16 m/s (Fig. 4a, Table 1) with wind gusts

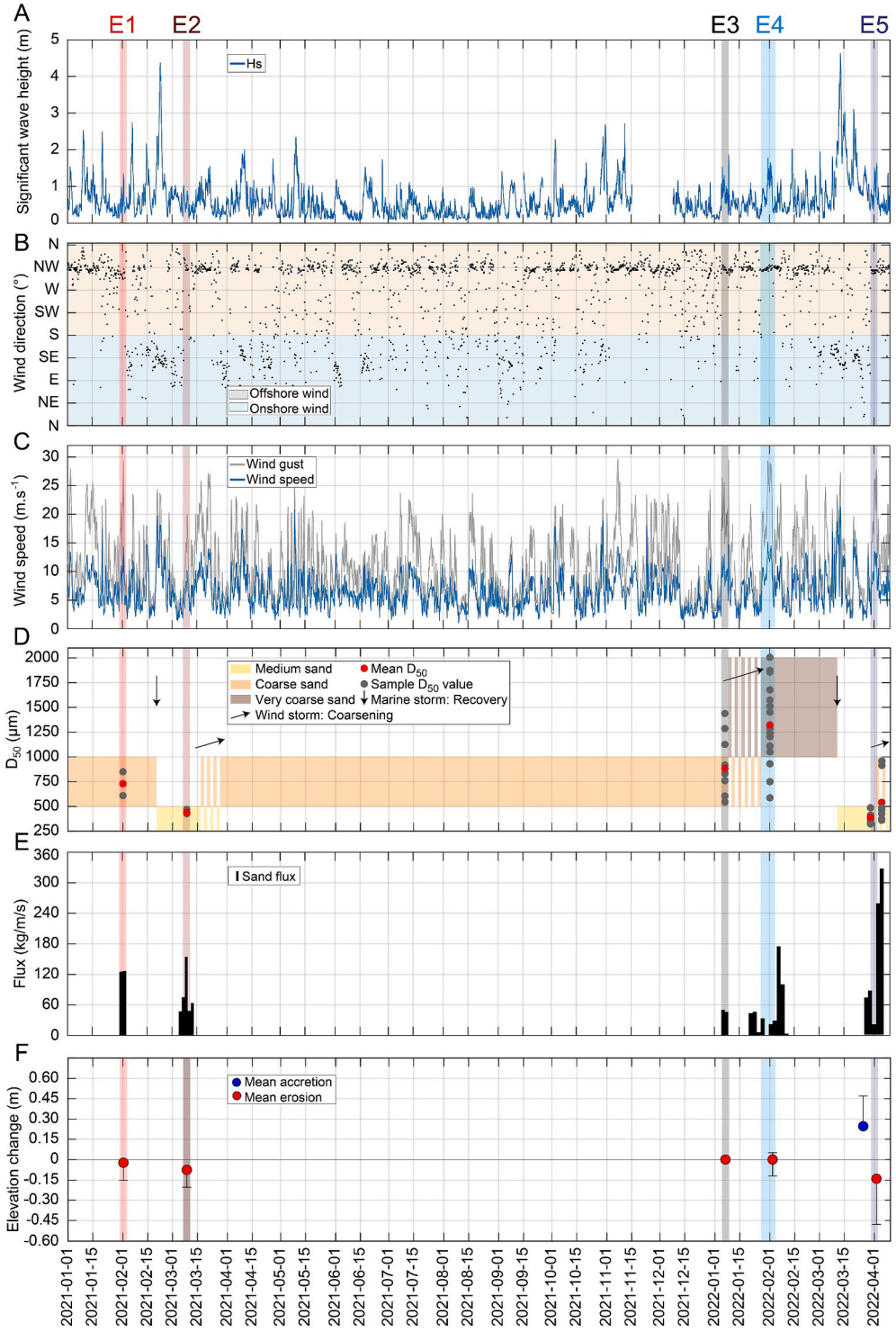

Fig. 3. (a) Overview of the wave height. (b) Wind direction and (c) wind speed from the Météo-France weather station in Cape-Leucate. (d) Granulometry characteristics of the beach and D_{50} of the beach surface sample. (Red circles the mean D_{50} per event and the grey ones D_{50} of all the beach surface sample). The coloured bars are the result of visual observation in the field and interpretation based on wind and wave conditions. (e) Observed sand flux (the bar chart widths are not to scale) during the events. (f) Mean vertical elevation change between the beginning to the end of the events (in red mean erosion and in blue mean accretion, the intervals give the maximum erosion or accretion).

up to 29 m/s. For E2 the five sand transport runs were measured during lower windspeed conditions, between 11 and 13 m/s (Fig. 4b, Table 1) with wind gusts up to 20 m/s. For E3, during R8 and R9, the wind speeds averaged 13 m/s and the wind gusts reached 23 m/s (Fig. 4b, Table 1). During the ten sand transport runs of E4 (R10 to R19), the wind characteristics were variable, averaging between 11 m/s and 16 m/s (Fig. 4d), with maximum gusts between 19 and 26 m/s. For the last event, E5, the sand transport runs conducted on 2022/03/31 occurred during moderate wind speeds ranging from 10 to 12 m/s, but the two runs carried out on 2022/04/01 had higher winds speed, above 15 m/s (Fig. 4e) with wind gusts up to 27 m/s.

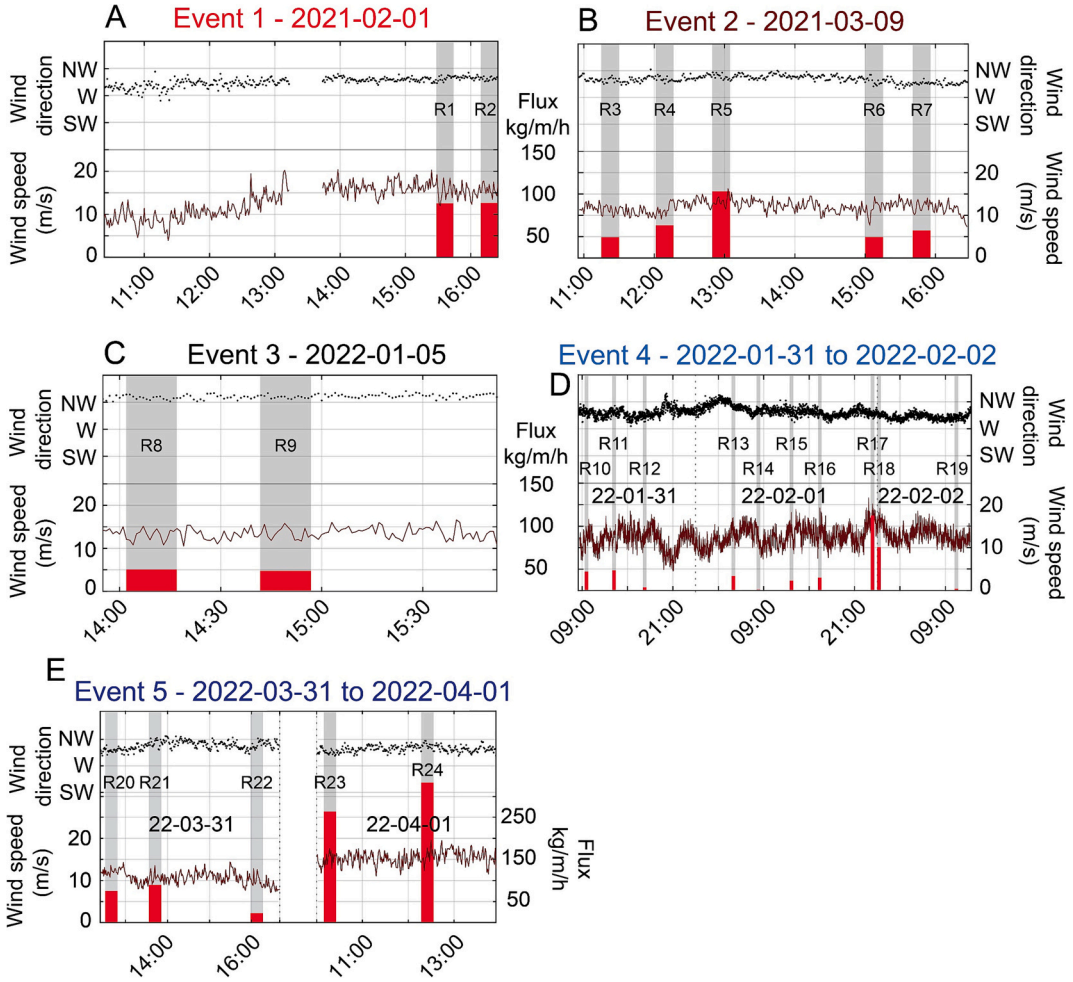

Fig. 4. Wind speed and wind direction at the dune crest station (2 m height) during each run ("R") per event with sand transport illustrated by the bar chart (their widths are at the right time scale).

4.2. Topographic evolution

In this section, the topographical changes (erosion and accretion) refer to vertical changes in elevation. The largest topographic change during E1 (interval of 6 h) occurred on the berm (erosion up to 0.15 m) and on the backshore (erosion between 0.05 m to 0.10 m). The average erosion of the topographic profile was 0.04 m (Fig. 5a). During E2 (interval of 6.5 h), erosion of 0.10 m to 0.20 m was observed on the berm and 0.05 to 0.08 m over the backshore with an average erosion along the profile of 0.074 m (Fig. 5b). Both events recorded accretion of <0.1 m on the beach face. During E3, no significant morphological change was observed (averaged erosion of the profile of 0.01 m), except on the beach face and swash zone with accretion of 0.1 to 0.3 m (Fig. 5c). For E4, erosion between 0.05 and 0.09 m was observed at the dune toe and slight accretion was measured on the beach of around 0.05 m (Fig. 5d). However, the average topographic change along the profile was close to zero. The marine storms that occurred between E4 and E5 (from 2022/03/12 to 2022/03/21), resulted in accretion of 0.5 m on the berm crest and between 0.1 and 0.4 m on the backshore (Fig. 5e) with an averaged accretion along the profile of 0.25 m. For E5 substantial topographic changes were observed with erosion of 0.55 m on the berm crest and erosion of 0.2 m on the backshore. On average, the profile eroded 0.13 m. The beach face and the swash zone/intertidal region, gained sediment, resulting in the coastline migrating seaward by about 5 m. During E5, the presence of three zones of woody debris on the backshore at the location of the wrack lines due to the marine storm between E4 and E5, acted as a protection against wind erosion.

4.3. Grain size analysis

The median grain size of the dune (called "dune zone" in Fig. 2) was constant over the annual scale (medium sand between 390 and 430 μm) unlike the beach which showed strong temporal variability. The D_{50} of the beach is indicated by a single averaged value based on all the samples taken across the beach profile during each event ("Mean D_{50} Event" in Fig. 6a), from the berm crest trapping station to the dune toe ("zone 1" in Fig. 2). During E1, the beach was characterized by coarse sand (D_{50} = 729 μm (609 to 850 μm)) as during E3 (D_{50} = 883 μm (719 to 1438)), and very coarse sand during E4 (D_{50} = 1323 μm (970 to 1707 μm), Fig. 6a). E2 and E5 had a lower D_{50}, composed of medium sand (respectively D_{50} = 439 (415 to 471) μm and 388 μm (342 to 428 μm), Fig. 6a). All samples (except after a marine storm, e.g. E5) were bimodal in size (two peaks in the size classification), and a variability of the magnitude of their fine and coarse modes was observed. For example, E4 samples (very coarse beach grain size) have a first dominant mode of very coarse sand (1250 μm, Fig. 6b) and a second of medium sand (250 μm, Fig. 6b). At the beginning of E5, the particle size classes were clearly unimodal, with a medium sand mode at 350 μm (Fig. 6b), but after 40 h of windstorm the post-E5 samples showed initialization of beach surface coarsening (Fig. 6a) with the appearance of a second mode of very coarse sand (1250 μm, Fig. 6b) in addition to its dominant mode of medium sand (350 μm, Fig. 6b). Finally, Fig. 7b-c illustrates the wide range of surface sand grain size that can occur during a two-month interval on the beach (E4 (very coarse sand) and E5 (medium sand)).

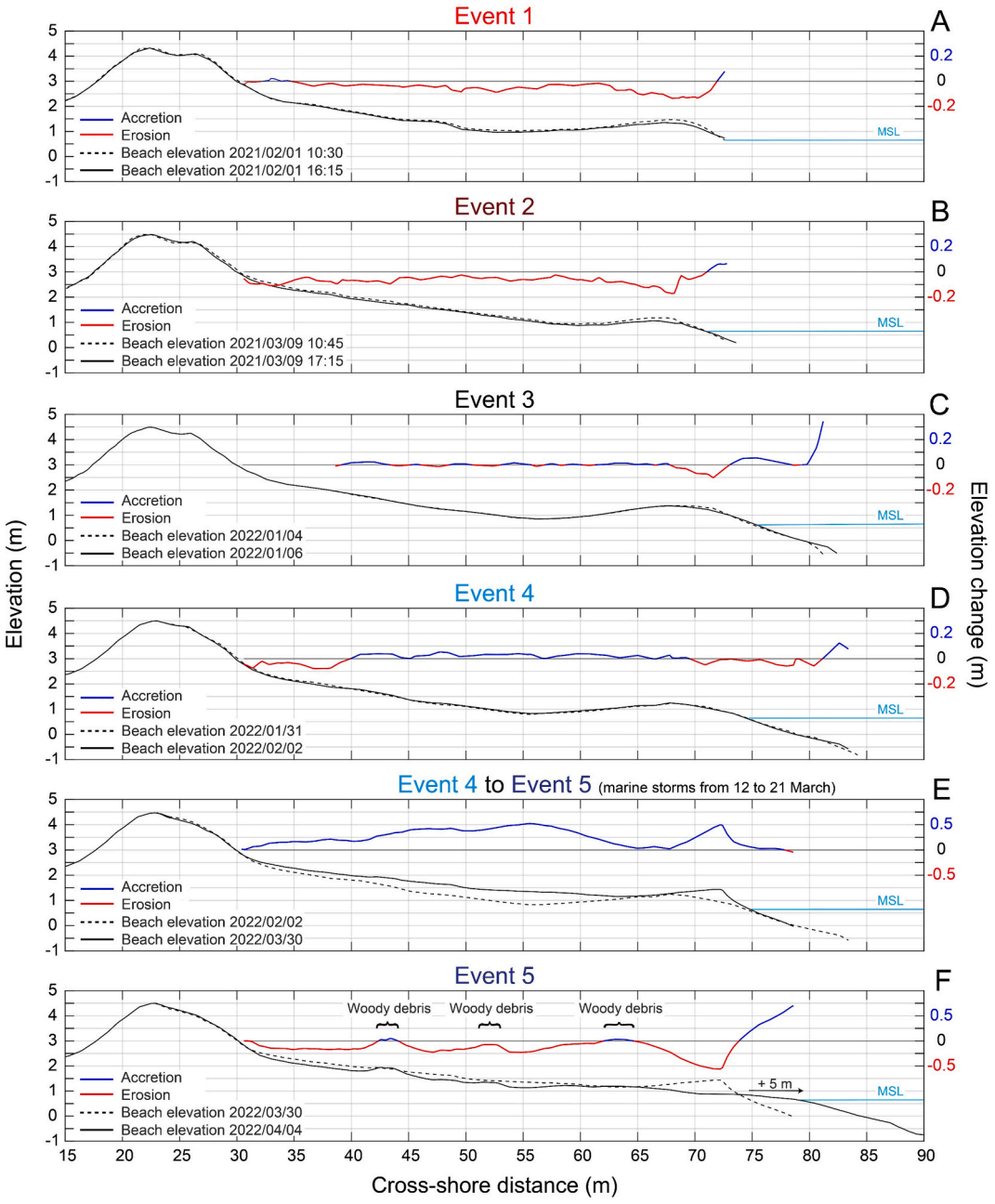

Fig. 5. (a, b, c, d, f) Topographic evolution during all events and (e) between the end of Event 4 and just before the Event 5 wind storm. (f) "MSL" is the Mean Sea Level measured in Port la Nouvelle tide gauge (13 km from the north of the study site). The arrow shows the seaward advance of the shoreline.

4.4. Sand flux

Beach moisture at the start of each wind event showed low values of <1 % except for E2 (1.8 %). For E5 surface moisture during the event was not measured, but the beach surface was visually observed as dry, however, rapid aeolian sediment erosion revealed moisture patches on the beach (Fig. 7c). The integrated sand flux data are summarized in Fig. 8. For E1 both transport runs were quite similar with high sand flux values about 125 and 126 kg/m/h and high wind speed. u_{*t} was exceeded for the entire run time during R2 (98% for R1 and 100 % for R2, Fig. 8). During E2 the five transport runs had medium to high sand fluxes, between 47 and 154 kg/m/h, and u_{*t} was exceeded between 88 % to 99 % of the time (Fig. 8). For E3 the two transport runs recorded medium values of sand transport around 50 kg/m/h and 78 % of the run was above u_{*t} (Fig. 8). The values of the ten transport runs during E4 were dominated by low sediment transport <10 kg/m/h and winds speeds predominantly below u_{*t}. Runs 17 and 18 recorded were exceptional in E4, with substantially higher rates of transport (174 and 100 kg/m/h respectively) and an increase in above u_{*t} winds to approximately about 80 % of each run (Fig. 8). The last campaign, E5, had similar wind speeds compared to E1 but lower than E4 and it has nevertheless recorded the highest sand transport rates between 258 and 326 kg/m/h despite high erosion rates revealing patches of moisture on the beach surface (Fig. 7c). The time above u_{*t} was at or close to 100 % for all runs during E5 except for R22 where is dropped to 87 %.

A

Event \ D_{50} (µm)	D_{50} Zone 1	D_{50} Zone 2	D_{50} Zone 3	D_{50} Zone 4	D_{50} Zone 5	D_{50} Zone 6	Mean D_{50} Event
Event 1			850 n=1		609 n=1		729 n=2
Event 2			415 n=1		431 n=1	471 n=1	439 n=3
Event 3	1022 n=2	839 n=2	763 n=2	796 n=2	719 n=2	1438 n=1	883 n=11
Event 4	1180 n=3	1164 n=3	1677n=1	970 n=3	1242 n=1	1707 n=5	1323 n=16
Event 5	410 n=1	408 n=3	381 n=2	429 n=2	342 n=2	360 n=2	388 n=12
Post-Event 5	462 n=1	948 n=1	355 n=1	345 n=1	426 n=1	646 n=2	547 n=7

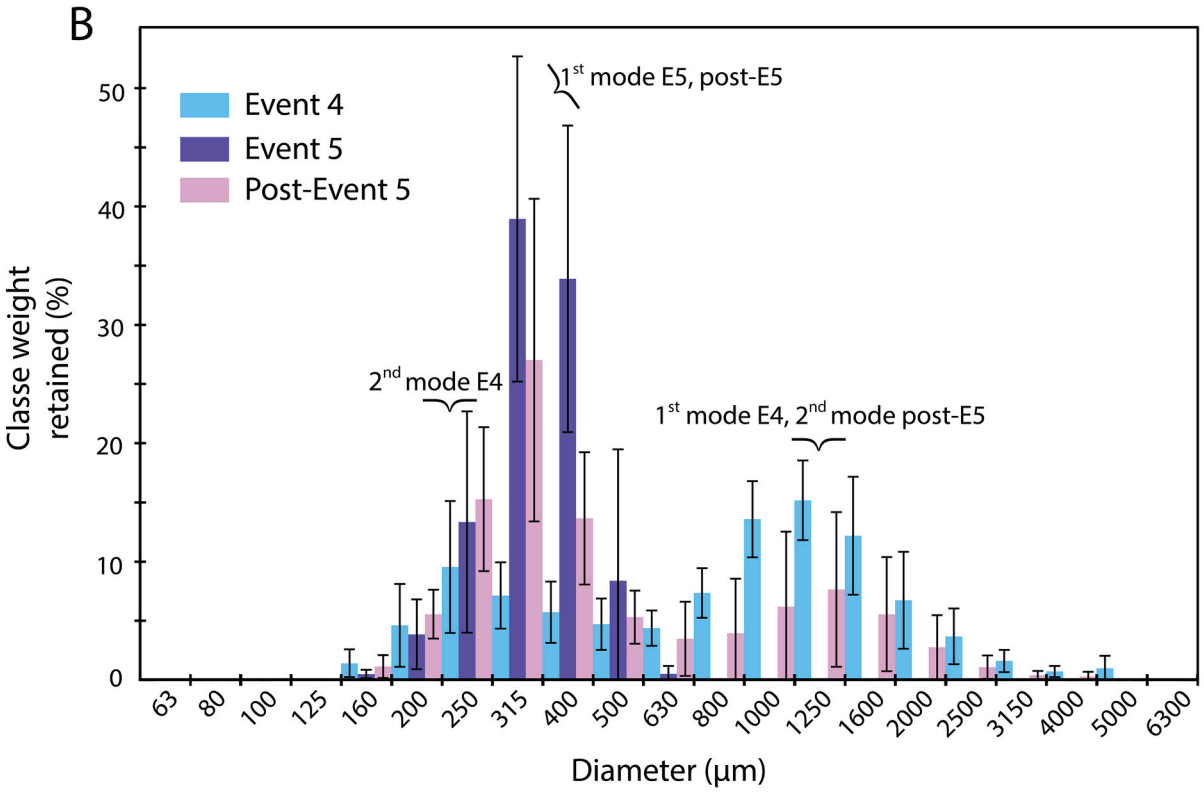

Fig. 6. (a) Mean D_{50} for each cross-shore zone, the "Mean D_{50} event" was calculated with all the dataset, not by the mean D_{50} of the different zone. (b) histogram of event 4 the coarser beach granulometry event, event 5 the finer one and post-event 5, after 40 h of windstorm. The histograms are the mean of each samples surface histogram for E4 ($n = 16$), E5 ($n = 12$) and post-E5 ($n = 7$). The error bar represents the standard deviation of the data.

5. Discussion

5.1. Relationship between observed aeolian sand transport and wind intensity

Aeolian sediment transport and wind speed were measured during five offshore wind events, representing a total of 24 runs. All measurements were made in dry weather conditions with a dry beach surface (moisture <2 %), removing the impact of surface moisture in the interpretation of the results, except at the end of E5. A wide range of transport rates was observed, ranging from <10 kg/m/h to 326 kg/m/h.

During an Event, values of sediment transport increased with wind speed in a linear fashion (Fig. 9). However, a correlation between sediment flux and wind speed at event scale was not always observed. In this study, we observed two types of relationships, one for medium sized sands (E2 and E5) and the other one for coarse and very coarse sands (E1, E3 and E4) (Fig. 9). The temporal evolution of beach grain size related to morphological beach state is a well-known relationship, already described elsewhere (e.g. Prodger et al., 2016; Van IJzendoorn et al., 2022), and is often related to hydrodynamic seasonality (Prodger et al., 2016, 2017; Medina et al., 1994). However, in this study, it is also related to the decoupling of marine and aeolian storms that play a key role in the temporal beach grain size variability. The observed coarsening of the beach induced by aeolian processes during periods of sustained above threshold winds is also reasonably well understood (Bagnold, 1937; Lancaster et al., 2002; Hoonhout and Vries, 2016; Field and Pelletier, 2018; Uphues et al., 2022; Cohn et al., 2022; Van IJzendoorn et al., 2022). However, the impact of grain size variability affecting the aeolian transport rates on the same beach is less known, especially from a quantitative point of view (Costas et al., 2020) and with such a broad range of grain sizes as observed in this study.

This study shows that for similar incident wind and climatic conditions, aeolian sediment transport rates can vary by over 1000 % depending on the granulometric state of the beach (Fig. 9). For example, during a wind speed of 12 m/s at 2 m height, the transport rates varied from 6 kg/m/h to 73 kg/m/h, with median beach grain sizes of 1323 µm and 388 µm respectively. When the wind increases in strength (e.g. 16 m/s), sand transport values can be >1.5 to 3 times higher, from 100 kg/

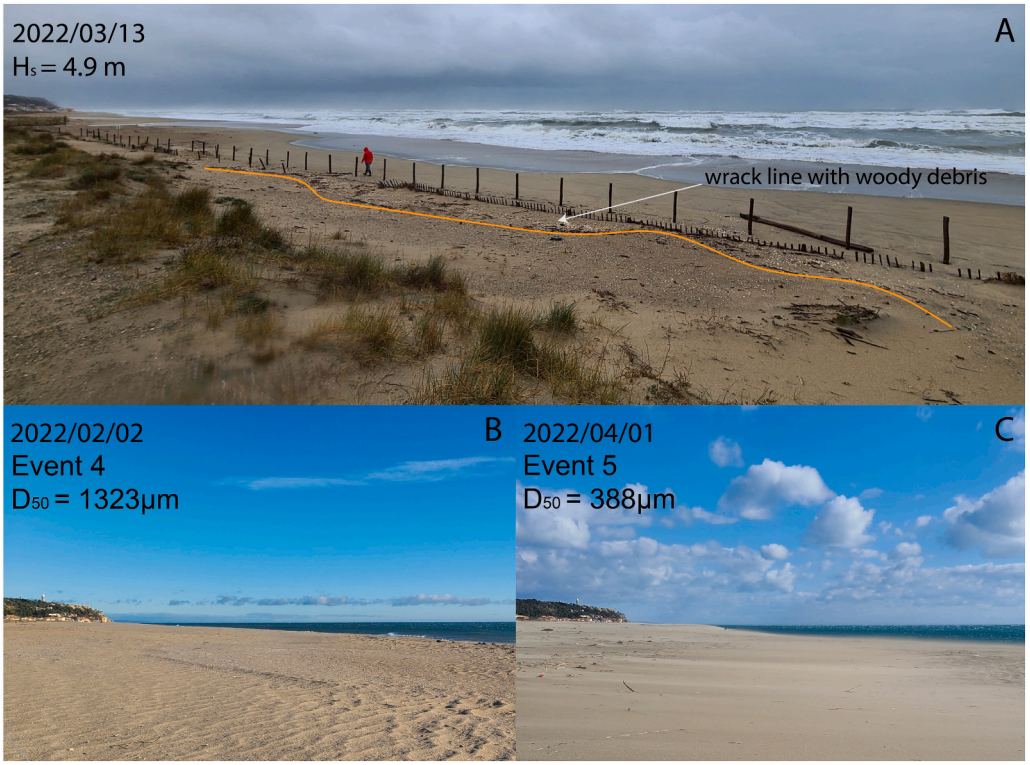

Fig. 7. (a) Ground photo of the beach during the marine storm before E5, the orange line shows the position of the wrack line. (b) Ground photo of the beach during E4 characterized by very coarse sand. (c) Ground photo of the beach during E5 with medium sand.

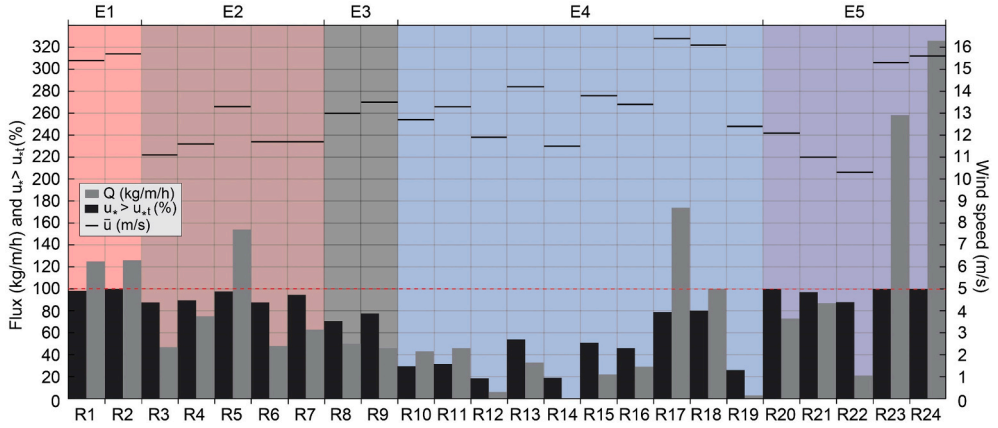

Fig. 8. Summary of the 24 sand transport runs. The bar chart in grey shows the sand transport flux and in black the percentage of the total run time (15 min) during which the shear velocity was above the threshold shear velocity (measured at the dune crest station). The dashed line represents the 100 % line which indicates that $u_* > u_{*t}$ for the whole 15 min run. The mean wind speed at the dune station during each run is shown by the horizontal line.

m/h to 326 kg/m/h for median beach grain sizes of 1323 µm and 388 µm respectively (Fig. 9). The time above the shear velocity threshold for each run shows that runs with coarse to very coarse grain size display less time above the threshold and weaker transport rates than runs with medium sand and similar wind speed. All these results demonstrate the importance of using an accurate D_{50} value when modelling sediment transport, even for beaches with multi-fractional sediments (Van Ijzendoorn et al., 2023). As these differences in transport rate were observed during offshore winds where the dune disturbs and reduces wind speed on the backshore (Walker and Nickling, 2002; Bauer et al., 2012; Delgado-Fernandez et al., 2013; Hesp et al., 2015; Smyth and Hesp, 2015; Hilton et al., 2016; Davidson et al., 2022), it is hypothesised differences between transport rates for medium and coarse sand could be even larger under onshore winds, where winds will be less variable and closer to a logarithmic boundary layer (Hesp and Smyth, 2016).

5.2. *Aeolian vs hydrodynamic processes affecting aeolian sediment transport*

In meso- to macrotidal environments, a large part of the beach is regularly flooded by the tide, allowing waves to mix sediments on the beach surface, resulting in a relatively homogenised and constant beach grain size (Reniers et al., 2013; Srisuwan et al., 2015). However, in microtidal environments, this process is limited, and waves only mix sediment during marine storms when the surge is sufficient (Hs ≥4 m at Leucate). Thus, wind processes are the most frequent driver of sediment sorting, and result in a coarsening of the beach's sediment that eventually results in a decrease of sediment transport flux (Lancaster et al.,

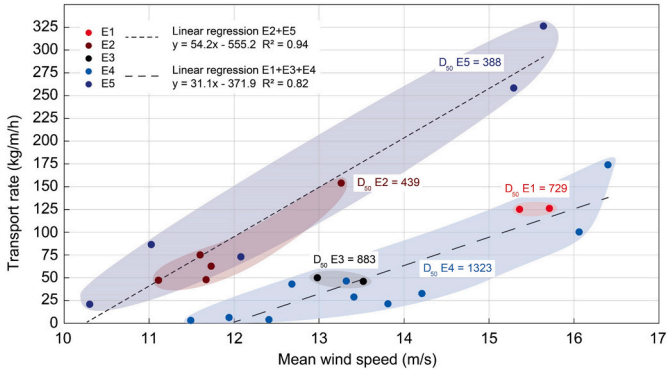

Fig. 9. Distribution of the transport rates for all the transport runs related to the mean wind speed at the dune station (2 m) for each 15 min run. The linear regressions were calculated with two families of beach grain size, the Events with medium sand (E2 and E5) and the events with coarse to very coarse sand (E1, E3 and E4). The median beach grain size (D_{50}) in μm was written with the numbers for each Event.

2002; Field and Pelletier, 2018; Cohn et al., 2022; Uphues et al., 2022). This behaviour is observed in the present study where over two days a medium-sized sandy beach (E5, D_{50} = 388 μm) became a coarse-sized beach (Post-E5, D_{50} = 545 μm). On longer time scales (weeks to months) these variabilities are even more accentuated, as beach sediments changed from medium sand (E2, D_{50} = 439 μm) to coarse sand (E3, D_{50} = 883 μm) and then to very coarse sand (E4, D_{50} = 1323 μm). The longer and stronger the wind blows, the greater the sediment sorting will be, to a point where only very coarse sediment remains and further aeolian sorting is only possible during extreme wind conditions. This coarsening is accompanied with an increase of the mean D_{50} of the beach and modification of the size class distribution. When the sand is composed of medium sand, the size classes were homogeneous and unimodal (mode at 315 μm, E5 in Fig. 6b) while with coarse to very coarse beach sand (E4 and post-E5 in Fig. 6b) a second additional very coarse mode at 1250 μm appears. The occurrence of this coarse mode is due to the prevalent transport of the finer sediment by the wind that make coarser the beach sediment. The bimodal distribution could also be explained by the erosion of finer sediment by the wind which exposes coarse layers that were previously buried (Gallagher et al., 2016).

As observed by Feyssat et al. (2022), the aeolian sand transport at Leucate is mainly caused by dry offshore winds, because onshore winds are often accompanied by humidity, rainfall and high wave runup that reduces the subaerial beach width and, thus, the fetch length (Bauer and Davidson-Arnott, 2003; Costas et al., 2020). However as observed in this study, marine processes can also have a significant impact on aeolian sand transport: 1) Depending on the wave energy and the tidal range conditions, the beach can be affected by spatially and temporally variable ranges of aeolian/hydrodynamic processes. In micro tidal areas more generally, the wind processes could affect the beach over a larger beach width and for longer periods of time, which might cause the effect of marine storms on the beach characteristics and thus on aeolian sediment transport to be more pronounced when they occur. 2) As shown in this study, in terms of beach sediment supply (Cohn et al., 2018; Pellón et al., 2020), it can be observed that during medium to high energy wave storms, the fine sand fraction is restored, sediment size is homogenised and beach accretion occurs (Eichentopf et al., 2019; Van IJzendoorn et al., 2022). This new, well mixed medium sand covers the previous beach surface by preserving the precedent coarse beach surface. Thus, this study confirms that the variability of aeolian transport rates is not only a function of wind intensity and other factors commonly listed in the literature such as fetch or humidity, but also hydrodynamic processes.

5.3. Impact of beach grain size variability on topographic evolution affected by aeolian sediment transport

Topographic change by aeolian processes is mostly documented for dune systems, rather than beaches (Hesp, 2002; Costas et al., 2020; Wiggs, 2022). In this study, significant vertical erosion (up to 0.55 m) was observed in a 40 h period of strong, offshore winds. Our results show that when the beach was composed of very coarse sand, offshore winds had little or no erosive effect (E3, Fig. 5c), even after two days of strong winds exceeding 25 m/s (E4, Fig. 5d). When the beach was composed of coarse sand as for E2, offshore winds had limited impact on the beach profile, resulting in erosion of <0.10 m (Fig. 5a). On the other hand, when the beach was composed of medium sand after high sediment supply by a marine storm, vertical erosion of 0.2 m on the backshore and up to 0.55 m on the crest of the berm was measured (E5, Fig. 5f). As winds were offshore, eroded sand was deposited at the shoreline, and reworked by small waves (Hs <1 m) resulting in a 5 m progradation of the beach as also observed by (Feyssat et al., 2024). In these hydrodynamic conditions the observed shoreline progradation couldn't be explained by nearshore bar welding to the beach but only by the seawards export of aeolian sand to the shoreline. This study demonstrates that the capacity of the wind to erode the beach is not only related to its intensity or blowing time, but also to the beach grain size, where the finer the grain size of the beach, the greater the backshore topographical variations will be (Nickling and Davidson-Arnott, 1990; Dong and Qian, 2006; Wang et al., 2021; Uphues et al., 2022). This behaviour is exacerbated in microtidal areas, where the relatively small tidal range and the short period exposed to wave processes minimises beach profile variability by hydrodynamic processes (Masselink and Pattiaratchi, 2001).

5.4. Morphodynamic model of a microtidal beach with heterogeneous granulometry

Based on the results of this study, a conceptual model of the microtidal beach evolution impacted by high beach grain size variability is presented (Fig. 10). This conceptual model shows how winds may affect beach topography at different time scales depending on the sedimentological context.

In the present study, the threshold to 'reset' the sedimentological state of the beach was observed at a significant wave height of 4 m (Fig. 10e) making the beach sediment finer and unimodal (e.g., E4 to E5). This resulted in greater aeolian sediment transport when the now lower threshold shear velocity was exceeded. This sedimentological state of medium sand was brief (hours to days), as medium sand was rapidly eroded during above threshold winds (e.g. post-E5, Fig. 6a). As finer sized sediment is eroded the period of time for continued coarsening to occur increased as the sediment threshold velocity increases (Fig. 10c-d). This process also explains why even with strong winds the topographic changes are limited when grain sizes are coarse or very coarse. The microtidal characteristics of the field site meant that hydrodynamic processes affecting the sediment mixing and inducing onshore sediment supply to the beach occurred only for a few days per year during winter marine storms (two storms with Hs up to 4 m were observed during the survey, Fig. 3). The rest of the time, the dominant dry offshore wind (71.6 % of the time) exported sand seaward. The sequence of this conceptual model is observed twice during the environmental monitoring (2021/01/01 to 2021/02/22 and 2021/02/22 to 2022/03/11).

Although this study was based on five field campaigns, and provided a comprehensive understanding of the causes of the grain size variability on a microtidal beach, several areas of future research remain, for example: 1) Better identification of the temporal beach grain size variability especially in the first hours to days during a wind event after the beach is 'reset' by marine processes. Sediment erosion in this period is rapid and higher temporal grain size measurements would help to

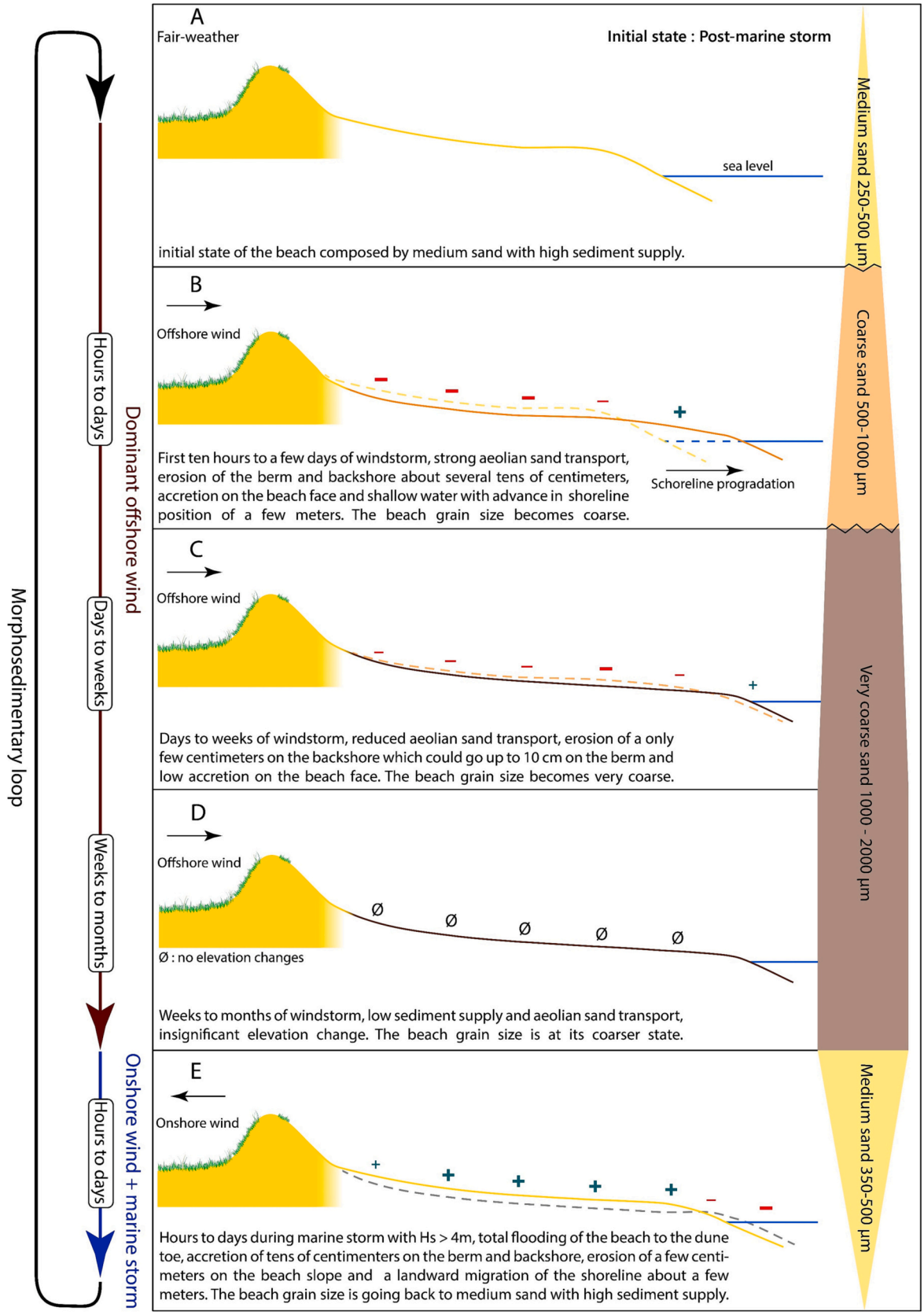

Fig. 10. Conceptual model of a microtidal beach influenced by an offshore wind. (a) Initial state. Step. (b, c and d) Offshore wind blows from several hours to few months thus coarsening the beach grain size, decreasing aeolian sand transport and decreasing topographic erosion over time. (e) Illustrates the return of sediment following a strong marine storm (Hs < 4 m) and flooding of the beach, sediment returns to a medium sand.

improve the understanding of temporal grain size transitions shown in Fig. 3d; 2) Impact of the water table on the aeolian sediment transport. In this study, its role is identified only during the end of E5 (medium sand, high transport rate). However, the variability of the water table may occur at other times following heavy rains, or in environments with greater temporal variability; 3) How storm magnitude impacts sediment mixing and beach sediment supply. Although the evolutionary mechanisms illustrated in the conceptual model were observed twice during the annual survey, the impact may vary with marine storm intensity. Thus, a small marine storm (2 m < Hs < 4 m) may only bring finer sand to part of the beach and in this case the backshore could present two very different beach surface characteristics, one with heterogeneous sand sorted by the wind (upper part), and the other with well sorted medium sand (lower part); 4) Finally, improved quantitative knowledge of sediment exchange processes between shallow marine and intertidal/terrestrial beaches. This will further our understanding of the net balance between sediment being deposited in shallow water during offshore events and sediment deposition on the beach during low-moderate swell and storm conditions. Future research might shed more light on this and could be conducted, for example, with fluorescent sand tracers (Robin et al., 2009; Suzuki et al., 2019).

6. Conclusion

Leucate beach (SE France) provides an example of a microtidal beach influenced by strong offshore winds and a high temporal variability of median sediment grain size. Five field campaigns with aeolian sand transport measurements, sedimentological samples and topographic data were carried out between 2021/01/01 to 2022/04/04. These experiments provide novel and quantitative insights into the morphodynamics of this coastal environment, particularly a better understanding of the influence of temporal grain size variability on aeolian sediment transport and topographic evolution. The results show that:

1. The subaerial grain size characteristics on a microtidal beach are highly variable and become progressively coarser due to aeolian erosion, changing from medium sand, to coarse sand and very coarse sand.
2. The linear relationship between sediment transport and wind speeds dramatically varies with beach grain size. This study found that during similar wind conditions when the sediment size was medium, sediment flux >1000 % greater than when beach sediments were coarse or very coarse. This demonstrates that the inherited sedimentological framework (e.g., beach grain size and sediment supply) variability in this type of environment can significantly influence aeolian transport rates regardless of wind intensity.
3. Only marine storms with a Hs > 4 m allowed for the return of fine sediment to the whole beach. The grain size of the beach was therefore regulated by the decoupling between the export of the finest sediment during offshore winds and their return during marine storms. This beach behaviour has a frequency that can be variable (smaller scale to seasonal) depending on large-scale climatic conditions (positioning of atmospheric low-pressure systems).
4. Sediment size strongly controls aeolian topographic beach change. The larger the grain size, the more it will act as an armouring layer and limit topographic changes. In this study offshore winds resulted in sediment deposition in the swash zone and lateral accretion of the shoreline when the beach was composed of medium sized sand. Little to no topographic change took place when the beach surface was comprised of coarse and very coarse sediment.

Further research should be conducted to determine the appropriate temporal and spatial resolution of sedimentological measurements on beaches to ensure that they are relevant considering the possible wide range of temporal or long-shore/cross-shore variations in the sedimentological characteristics in this type of environment. Similarly, these results need to be compared and put in the context of onshore-wind dominated microtidal environments.

CRediT authorship contribution statement

Antoine Lamy: Conceptualization, Data curation, Formal analysis, Methodology, Visualization, Writing – original draft, Writing – review & editing. **Nicolas Robin:** Conceptualization, Methodology, Writing – original draft, Writing – review & editing. **Thomas A.G. Smyth:** Conceptualization, Writing – review & editing. **Patrick A. Hesp:** Conceptualization, Writing – review & editing. **Camille René:** Methodology. **Pierre Feyssat:** Methodology. **Olivier Raynal:** Methodology. **Bertil Hebert:** Methodology.

Declaration of competing interest

The authors declare that they have no known competing financial interests or personal relationships that could have appeared to influence the work reported in this paper.

Data availability

Data will be made available on request.

Acknowledgements

The authors thank Obscat and the Parc Naturel Marin du Golfe du Lion for their financial support. The corresponding author is funded through a ministerial PhD grant from the French government. The authors thank Météo-France for supplying meteorological data, CANDHIS/CEREMA for wave data and all the contributors to the fieldwork. The authors would like to thank the editor-in-chief, C. Van Ijzendoorn and anonymous reviewers who helped to improve this article.

References

Aleman, N., Robin, N., Certain, R., Vanroye, C., 2011. Typology of nearshore bars in the Gulf of Lions (France) using LIDAR technology. J. Coast. Res. SI 64, 721–725.
Aleman, N., Robin, N., Certain, R., Anthony, E.J., Barusseau, J.-P., 2015. Longshore variability of beach states and bar types in a microtidal, storm-influenced, low-energy environment. Geomorphology 241, 175–191. https://doi.org/10.1016/j.geomorph.2015.03.029.
Arens, S.M., Baas, A.C.W., Van Boxel, J.H., Kalkman, C., 2001. Influence of reed stem density on foredune development. Earth Surf. Process. Landf. 26, 1161–1176. https://doi.org/10.1002/esp.257.
Bagnold, R.A., 1937. The transport of sand by wind. Geogr. J. 89, 409–438. https://doi.org/10.2307/1786411.
Bascom, W.N., 1951. The relationship between sand size and beach-face slope. Trans. Am. Geophys. Union 32, 866. https://doi.org/10.1029/TR032i006p00866.
Bauer, B.O., Davidson-Arnott, R.G.D., 2003. A general framework for modeling sediment supply to coastal dunes including wind angle, beach geometry, and fetch effects. Geomorphology 49, 89–108. https://doi.org/10.1016/S0169-555X(02)00165-4.
Bauer, B.O., Davidson-Arnott, R.G.D., 2014. Aeolian particle flux profiles and transport unsteadiness: aeolian particle flux profiles. Case Rep. Med. 119, 1542–1563. https://doi.org/10.1002/2014JF003128.
Bauer, B.O., Davidson-Arnott, R.G.D., Hesp, P.A., Namikas, S.L., Ollerhead, J., Walker, I. J., 2009. Aeolian sediment transport on a beach: surface moisture, wind fetch, and mean transport. Geomorphology 105, 106–116. https://doi.org/10.1016/j.geomorph.2008.02.016.
Bauer, B.O., Davidson-Arnott, R.G.D., Walker, I.J., Hesp, P.A., Ollerhead, J., 2012. Wind direction and complex sediment transport response across a beach-dune system. Earth Surf. Process. Landf. 37, 1661–1677. https://doi.org/10.1002/esp.3306.
Buckley, R., 1987. The effect of sparse vegetation on the transport of dune sand by wind. Nature 325, 426–428. https://doi.org/10.1038/325426a0.
Bujan, N., Cox, R., Masselink, G., 2019. From fine sand to boulders: examining the relationship between beach-face slope and sediment size. Mar. Geol. 417, 106012 https://doi.org/10.1016/j.margeo.2019.106012.
Carter, R.W.G., 1976. Formation, maintenance and geomorphological significance of an aeolian shell pavement. JSR 46. https://doi.org/10.1306/212F6F8C-2B24-11D7-8648000102C1865D.
Cerema, Dreal, L.R., 2019. Observatoire Océanologique de Banyuls CANDHIS—Détail de La Campagne 01101—Leucate. Available online. https://candhis.cerema.fr/_public_/campagne.php.

Certain, R., 2002. Morphodynamique d'une côte Sableuse Microtidale à Barres: Le Golfe du Lion (Languedoc-Roussillon). Ph.D. thesis Thèse. Université de Perpignan, Perpignan, France.
Cohn, N., Ruggiero, P., Vries, S., Kaminsky, G., 2018. New insights on coastal foredune growth: the relative contributions of marine and aeolian processes. Geophys. Res. Lett. 45 https://doi.org/10.1029/2018GL077836.
Cohn, N., Dickhudt, P., Marshall, J., 2022. In-situ measurement of grain size characteristics within the aeolian saltation layer on a coastal beach. Earth Surf. Process. Landf. 47, 2230–2244. https://doi.org/10.1002/esp.5373.
Costas, S., de Sousa, L.B., Kombiadou, K., Ferreira, Ó., Plomaritis, T.A., 2020. Exploring foredune growth capacity in a coarse sandy beach. Geomorphology 371, 107435. https://doi.org/10.1016/j.geomorph.2020.107435.
Davidson, S.G., Hesp, P.A., DaSilva, M., Da Silva, G.M., 2022. Flow dynamics over a high, steep, erosional coastal dune slope. Geomorphology 402, 108111. https://doi.org/10.1016/j.geomorph.2022.108111.
Davidson-Arnott, Law, 1990. Seasonal patterns and controls on sediment supply to coastal foredunes, Long Point, Lake Erie. In: Nordstrom, K.F., Psuty, N.P., Carter, R. W.G. (Eds.), Coastal Dunes: Form and Process. John Wiley and Sons, pp. 177–200.
de Vries, S., Southgate, H.N., Kanning, W., Ranasinghe, R., 2012. Dune behavior and aeolian transport on decadal timescales. Coast. Eng. 67, 41–53. https://doi.org/10.1016/j.coastaleng.2012.04.002.
de Vries, S., Arens, S.M., de Schipper, M.A., Ranasinghe, R., 2014. Aeolian sediment transport on a beach with a varying sediment supply. Aeolian Res. 15, 235–244. https://doi.org/10.1016/j.aeolia.2014.08.001.
Delgado-Fernandez, I., 2010. A review of the application of the fetch effect to modelling sand supply to coastal foredunes. Aeolian Res. 2, 61–70. https://doi.org/10.1016/j.aeolia.2010.04.001.
Delgado-Fernandez, I., Jackson, D.W.T., Cooper, J.A.G., Baas, A.C.W., Beyers, J.H.M., Lynch, K., 2013. Field characterization of three-dimensional lee-side airflow patterns under offshore winds at a beach-dune system. Case Rep. Med. 118, 706–721. https://doi.org/10.1002/jgrf.20036.
Dong, Z., Qian, G., 2006. Characterizing the height profile of the flux of wind-eroded sediment. Environ. Geol. 51, 835–845. https://doi.org/10.1007/s00254-006-0363-5.
Dong, Z., Liu, X., Wang, X., 2002. Wind initiation thresholds of the moistened sands. Geophys. Res. Lett. 29, 1585. https://doi.org/10.1029/2001GL013128.
Eichentopf, S., van der Zanden, J., Cáceres, I., Alsina, J.M., 2019. Beach profile evolution towards equilibrium from varying initial morphologies. J. Mar. Sci. Eng. 7, 406. https://doi.org/10.3390/jmse7110406.
Ellis, J.T., Li, B., Farrell, E.J., Sherman, D.J., 2009. Protocols for characterizing aeolian mass-flux profiles. Aeolian Res. 1, 19–26. https://doi.org/10.1016/j.aeolia.2009.02.001.
Ferrer, P., Certain, R., Barusseau, J.-P., Gervais, M., 2010. Modélisation conceptuelle d'un littoral à double barre festonnée en milieu microtidal. In: XIèmes Journées, Les Sables d'Olonne. Presented at the Journées Nationales Génie Côtier - Génie Civil, Editions Paralia, pp. 235–242. https://doi.org/10.5150/jngcgc.2010.029-F.
Feyssat, P., Certain, R., Robin, N., Raynal, O., Aleman, N., Hebert, B., Lamy, A., Barusseau, J.-P., 2022. Morphodynamic behaviour of a mediterranean intermittent estuary with opening phases primarily dominated by offshore winds. J. Mar. Sci. Eng. 10, 1817. https://doi.org/10.3390/jmse10121817.
Feyssat, P., Certain, R., Robin, N., Barusseau, J.-P., Lamy, A., Raynal, O., Hebert, B., 2024. Morphodynamics of two Mediterranean microtidal beaches presenting permanent megacusps under the influence of waves and strong offshore winds. Cont. Shelf Res. 272, 105160 https://doi.org/10.1016/j.csr.2023.105160.
Field, J.P., Pelletier, J.D., 2018. Controls on the aerodynamic roughness length and the grain-size dependence of aeolian sediment transport. Earth Surf. Process. Landf. 43, 2616–2626. https://doi.org/10.1002/esp.4420.
Gallagher, E., Wadman, H., McNinch, J., Reniers, A., Koktas, M., 2016. A conceptual model for spatial grain size variability on the surface of and within beaches. J. Mar. Sci. Eng. 4, 38. https://doi.org/10.3390/jmse4020038.
Hallin, C., IJzendoorn, C.V., Homberger, J.-M., De Vries, S., 2023. Simulating surface soil moisture on sandy beaches. Coast. Eng. 185, 104376 https://doi.org/10.1016/j.coastaleng.2023.104376.
Hardisty, J., Whitehouse, R.J.S., 1988. Evidence for a new sand transport process from experiments on Saharan dunes. Nature 332, 532–534. https://doi.org/10.1038/332532a0.
He, Y., Liu, J., Cai, F., Li, B., Qi, H., Zhao, S., 2022. Aeolian sand transport influenced by tide and beachface morphology. Geomorphology 396, 107987. https://doi.org/10.1016/j.geomorph.2021.107987.
Hesp, P., 2002. Foredunes and blowouts: initiation, geomorphology and dynamics. Geomorphology 48, 245–268. https://doi.org/10.1016/S0169-555X(02)00184-8.
Hesp, P.A., 2024. Coastal dunes: types, initiation, morphology, evolution, and relationships to surfzone-beach systems and climate. In: Treatise on Estuarine and Coastal Science, 2nd edition. https://doi.org/10.1016/B978-0-323-90798-9.00074-3.
Hesp, P.A., Smyth, T.A., 2016. Surfzone-beach-dune interactions: flow and sediment transport across the intertidal beach and backshore. J. Coast. Res. 75, 8–12.
Hesp, P.A., Smyth, T.A.G., Nielsen, P., Walker, I.J., Bauer, B.O., Davidson-Arnott, R., 2015. Flow deflection over a foredune. Geomorphology 230, 64–74. https://doi.org/10.1016/j.geomorph.2014.11.005.
Hilton, M.J., Hatcher, S.V., Wakes, S.J., Konlechner, T.M., 2016. Flow deflection and deceleration across a simple foredune. J. Coast. Res. 75, 293–297. https://doi.org/10.2112/SI75-059.1.
Hilton, M., Nickling, B., Wakes, S., Sherman, D., Konlechner, T., Jermy, M., Geoghegan, P., 2017. An efficient, self-orienting, vertical-array, sand trap. Aeolian Res. 25, 11–21. https://doi.org/10.1016/j.aeolia.2017.01.003.
Hoonhout, B.M., Vries, S. de, 2016. A process-based model for aeolian sediment transport and spatiotemporal varying sediment availability. Case Rep. Med. 121, 1555–1575. https://doi.org/10.1002/2015JF003692.
Hsu, S.A., 1973. Computing eolian sand transport from shear velocity measurements. J. Geol. 81, 739–743. https://doi.org/10.1086/627927.
Huisman, B.J.A., de Schipper, M.A., Ruessink, B.G., 2016. Sediment sorting at the sand motor at storm and annual time scales. Mar. Geol. 381, 209–226. https://doi.org/10.1016/j.margeo.2016.09.005.
Lancaster, N., Nickling, W.G., McKenna Neuman, C., 2002. Particle size and sorting characteristics of sand in transport on the stoss slope of a small reversing dune. Geomorphology 43, 233–242. https://doi.org/10.1016/S0169-555X(01)00135-0.
Manukyan, E., Prigozhin, L., 2009. Formation of aeolian ripples and sand sorting. Phys. Rev. E 79, 031303. https://doi.org/10.1103/PhysRevE.79.031303.
Masselink, G., Pattiaratchi, C.B., 2001. Seasonal changes in beach morphology along the sheltered coastline of Perth, Western Australia. Mar. Geol. 172, 243–263. https://doi.org/10.1016/S0025-3227(00)00128-6.
Medina, R., Losada, M.A., Losada, I.J., Vidal, C., 1994. Temporal and spatial relationship between sediment grain size and beach profile. Mar. Geol. 118, 195–206. https://doi.org/10.1016/0025-3227(94)90083-3.
Mendoza, E.T., Jimenez, J.A., Mateo, J., 2011. A coastal storms intensity scale for the Catalan sea (NW Mediterranean). Nat. Hazards Earth Syst. Sci. 11, 2453–2462. https://doi.org/10.5194/nhess-11-2453-2011.
Moreira, M.E.S.A., 1988. Seasonal processes of the beach-dune system on the western coast of Portugal. J. Coast. Res. 47–51.
Mountney, N.P., Russell, A.J., 2009. Aeolian dune-field development in a water table-controlled system: Skeiðarársandur, Southern Iceland. Sedimentology 56, 2107–2131. https://doi.org/10.1111/j.1365-3091.2009.01072.x.
Namikas, S.L., 2003. Field Measurement and Numerical Modelling of Aeolian Mass Flux Distributions on a Sandy Beach, p. 24.
Nickling, W.G., Davidson-Arnott, R.G.D., 1990. Aeolian sediment transport on beaches and coastal sand dunes. In: Proc. Symposium Coastal Sand Dunes. Ottawa, pp. 1–35.
Nield, J.M., Wiggs, G.F.S., Squirrell, R.S., 2011. Aeolian sand strip mobility and protodune development on a drying beach: examining surface moisture and surface roughness patterns measured by terrestrial laser scanning. Earth Surf. Process. Landf. 36, 513–522. https://doi.org/10.1002/esp.2071.
Nikuradse, J., 1933. Stromungsgesetze in rauhen Rohren. vdi-forschungsheft, 361, p. 1.
Nordstrom, K.F., 1980. Cyclic and seasonal beach response: a comparison of oceanside and bayside beaches. Phys. Geogr. 1, 177–196. https://doi.org/10.1080/02723646.1980.10642199.
Pellón, E., de Almeida, L.R., González, M., Medina, R., 2020. Relationship between foredune profile morphology and aeolian and marine dynamics: a conceptual model. Geomorphology 351, 106984. https://doi.org/10.1016/j.geomorph.2019.106984.
Poortinga, A., Keijsers, J.G.S., Maroulis, J., Visser, S.M., 2014. Measurement uncertainties in quantifying aeolian mass flux: evidence from wind tunnel and field site data. PeerJ 2, e454. https://doi.org/10.7717/peerj.454.
Prodger, S., Russell, P., Davidson, M., Miles, J., Scott, T., 2016. Understanding and predicting the temporal variability of sediment grain size characteristics on high-energy beaches. Mar. Geol. 376, 109–117. https://doi.org/10.1016/j.margeo.2016.04.003.
Prodger, S., Russell, P., Davidson, M., 2017. Grain-size distributions on high-energy sandy beaches and their relation to wave dissipation. Sedimentology 64, 1289–1302. https://doi.org/10.1111/sed.12353.
Rasmussen, K.R., Mikkelsen, H.E., 1998. On the efficiency of vertical array aeolian field traps. Sedimentology 45, 789–800. https://doi.org/10.1046/j.1365-3091.1998.00179.x.
Reniers, A.J.H.M., Gallagher, E.L., MacMahan, J.H., Brown, J.A., van Rooijen, A.A., van Thiel de Vries, J.S.M., van Prooijen, B.C., 2013. Observations and modeling of steep-beach grain-size variability. J. Geophys. Res. Oceans 118, 577–591. https://doi.org/10.1029/2012JC008073.
Robin, N., Levoy, F., Monfort, O., 2009. Short term morphodynamics of an intertidal bar on megatidal ebb delta. Mar. Geol. 260, 102–120. https://doi.org/10.1016/j.margeo.2009.02.006.
Ruz, M.H., Anthony, E.J., 2008. Trapping by brushwood fences on a beach-foredune contact: the primacy of the local sediment budget. Z. Geomorphol. 52, 179–194.
Schmutz, P.P., Namikas, S.L., 2018. Measurement and modeling of the spatiotemporal dynamics of beach surface moisture content. Aeolian Res. 34, 35–48. https://doi.org/10.1016/j.aeolia.2018.08.001.
Schwarz, C., van Starrenburg, C., Donker, J., Ruessink, G., 2021. Wind and sand transport across a vegetated foredune slope. Case Rep. Med. 126 https://doi.org/10.1029/2020JF005732.
Smyth, T.A.G., Hesp, P.A., 2015. Aeolian dynamics of beach scraped ridge and dyke structures. Coast. Eng. 99, 38–45. https://doi.org/10.1016/j.coastaleng.2015.02.011.
Srisuwan, C., Work, P.A., Karasu, S., Özölçer, İ.H., 2015. Beach profile model with size-selective sediment transport. I: laboratory experiment and sensitivity study. J. Waterw. Port Coast. Ocean Eng. 141, 04014032 https://doi.org/10.1061/(ASCE)WW.1943-5460.0000255.
Strypsteen, G., van Rijn, L.C., Hoogland, M.D., Rauwoens, P., Fordeyn, J., Hijma, M.P., Lodder, Q.J., 2021. Reducing aeolian sand transport and beach erosion by using armour layer of coarse materials. Coast. Eng. 166, 103871 https://doi.org/10.1016/j.coastaleng.2021.103871.
Suzuki, T., Inami, Y., Yanagishima, S., Sakihama, S., Cox, D.T., 2019. Sediment particle movements observed using tracers under accretive wave conditions in the nearshore zone. Coast. Eng. J. 61, 472–485. https://doi.org/10.1080/21664250.2019.1629863.

Swann, C., Lee, D., Trimble, S., Key, C., 2021. Aeolian sand transport over a wet, sandy beach. Aeolian Res. 51, 100712 https://doi.org/10.1016/j.aeolia.2021.100712.
Uphues, C.F.K., van IJzendoorn, C.O., Hallin, C., Pearson, S.G., van Prooijen, B.C., da Silva, G.M., de Vries, S., 2022. Coastal aeolian sediment transport in an active Bed Surface Layer: tracer study and conceptual model. Earth Surf. Process. Landf. esp.5449 https://doi.org/10.1002/esp.5449.
Van der Wal, D., 1998. Effects of fetch and surface texture on aeolian sand transport on two nourished beaches. J. Arid Environ. 39, 533–547. https://doi.org/10.1006/jare.1997.0364.
Van IJzendoorn, C.O., Hallin, C., Cohn, N., Reniers, A.J.H.M., De Vries, S., 2022. Novel sediment sampling method provides new insights into vertical grain size variability due to marine and aeolian beach processes. Earth Surf. Process. Landf. esp.5518 https://doi.org/10.1002/esp.5518.
Van IJzendoorn, C.O., Hallin, C., Ad, R., Vries, S. de, 2023. Modeling Multi-fraction Coastal Aeolian Sediment Transport With Horizontal and Vertical Grain Size Variability (Preprint). Preprints. https://doi.org/10.22541/essoar.167898491.19162099/v1.
Walker, I.J., Nickling, W.G., 2002. Dynamics of secondary airflow and sediment transport over and in the lee of transverse dunes. Prog. Phys. Geogr. Earth Environ. 26, 47–75. https://doi.org/10.1191/0309133302pp325ra.
Wang, X., Zhang, C., Zou, X., 2021. A model of the sand transport rate that accounts for temporal evolution of the bed. Geomorphology 378, 107616. https://doi.org/10.1016/j.geomorph.2021.107616.
Wiggs, G.F.S., 2022. Dune morphology and dynamics. In: Treatise on Geomorphology. Elsevier, pp. 454–480. https://doi.org/10.1016/B978-0-12-818234-5.00073-0.
Wright, L.D., Short, A.D., 1984. Morphodynamic variability of surf zones and beaches: a synthesis. Mar. Geol. 56, 93–118. https://doi.org/10.1016/0025-3227(84)90008-2.